Emad S. Al-Hassani
Materials Engineering Department, University of Technology, Baghdad, Iraq
emad2000x@yahoo.com

Received on: 01/03/2017
Accepted on: 23/11/2017

Investigation of Microstructure and Chemical Analysis Along Weldments AISI 410 MSS/ER Nicrmo-3

Abstract-*In this research work the weldability of AISI 410 martensitic stainless steels (SS) LP-blades of steam turbine joined by GTAW (gas tungsten arc welding); inconel-3 filler wire was investigated. To study the mechanical performance and microstructural characteristics of the welded joint, the optical-microscopic and micro-hardness were applied along the cross-section of specimens, respectively. Line/Point and EDS technique were used to predict the chemical composition of welding joint. WDS MAP/ WDS LINK (Energy Dispersive Spectroscopy) used to know the movement of elements along the weldments. Results showed that micro-hardness along the HAZ regions increased. Microstructure photographs revealed γ-austenite as predominate phase along weld-metal. X-ray image with magnification 10μm showed two phases: dendritic (dark region) and interdendrite (light region) phases. Moreover, coarse grains appeared in HAZ zone of both weldments. In addition, chemical composition appeared carbon aggregated at interface.*

Keywords- *Turbine Blade, GTRW, Martensitic Stainless Steels, Filler Wire*

How to cite this article: E.S. Al-Hassani, "Investigation of Microstructure and Chemical Analysis Along Weldments AISI 410 MSS/ ER Nicrmo-3," *Engineering and Technology Journal*, Vol. 36, Part A, No. 5, pp. 564-573, 2018.

1. Introduction

Blades of steam turbine are stringent components in power plants. These blades converted the linear motion of the high temperature high-pressure (HP) steam flowing down a pressure gradient into a rotary motion of the turbine shaft at about 3000 rotations per minute (rpm) [1]. Generally, LP (low pressure) blades of a steam turbine are found to be more susceptible to failure more than the other types IP (intermediate pressure) and HP (high pressure) blades. The blades are subjected to high bending and centrifugal forces. 12% chromium martensitic steel is the most popular blade materials. It has an excellent combination of strength, toughness and corrosion resistance as well as high inherent damping characteristics [2]. Bhaduri et al. investigated the developed of welding repair procedure on cracked blades steam turbine was made from MSS (martensitic stainless steel) by using TIG (Tungsten Inert Gas) welding process and consumable filler wire as ER 316L austenitic filler wires and ER 410 MSS. Results showed that employing ER 410 filler wire with preheating and PWHT processes is appropriate to weld MSS blades turbine [3]. Divya et al. 2011 investigated the details in-situ repair welding of cracked shrouds of steam turbine and characterization of the welding joint. Shrouds crack of the 3rd stage of a LP turbine was in-situ repaired by taking off the pieces of crack of the shroud that made of AISI 414 martensitic stainless steel (MSS) and welding by using GTAW with ER 410NiMo consumable metal wire. Micro-hardness result showed weld-metal region in state as welded and after heat-treated was reduced from 400-260 VHN with applied load 500g [4]. Mithilesh et al. 2014 investigated the dissimilar welding joint by (GTAW) process with using ERNiCrMo-3 (Inconel-82). The dissimilar welding joints between AISI 304 and inconel 625 were studied. The investigated mechanical properties and microstructure characteristic of dissimilar welding. SEM /EDAX and optical microscopic (OP) analyze were employing to evaluate relationships of the structure property on these dissimilar weldments. It was found segregation or secondary phase's formation at the HAZ of AISI 304.Also, coarser grains were found at the HAZ region of AISI 304 [5]. Arivarasu et al. 2015 dissimilar welding joint between AISI 304L (ASS) and low alloyed AISI 4340 aeronautical steel that welded joint by CC (continuous current) and PC (pulsed current) GTAW techniques with using two types of consumables filler metal as ER309L and ERNiCr-3 were investigated. EDS/SEM analysis in case of CCGTA weldment showed a great amount of Fe element was diffused from AISI 4340 toward the weld-metal region, also, both Ni and Cr contents were found fewer diffused from weld-metal region toward

https://doi.org/10.30684/etj.36.5A.12
2412-0758/University of Technology-Iraq, Baghdad, Iraq

AISI 4340 side in both the welding processes. While in the case PCGTA weldments can be noted diffusion of elements is totally minimized so that negligible changes [6]. In this work, it has been investigated the weldability of LP-blades turbine made of AISI 410 martensitic stainless steels (SS). For this purpose, TIG (tungsten arc welding) and Ni-based alloys including ER NiCrMo-3 was implode as filler wire. The aim of this research is investigate the developing of repair welding procedure to repair steam turbine blades by using ER NiCrMo-3 and chemical composition along weldment AISI 410 MSS/ER NiCrMo-3.

2. Experimental Work

I. Base materials and procedure of welding

AISI 410 martensitic stainless steel was used as a base metal and filler metal employed in this study was ERNiCrMo-3 consumable filler wire, chemical composition of base and weld metals used in this research are given in Table 1, respectively. AISI 410 MSS blades were cutting by wire electrical discharge machine (EDM) to the pair's symmetry (each pair's has dimensioned approximately 25mm*100mm). Followed by, it is achieved standard V-Butt configurations (single V-groove having a root face of 2 mm and included angle of 70°). Figure 1 illustrates the schematic configuration of V-Butt welding joint. Multi-pass welding was performed through TIG welding machine (type/ ESAB LRT 160) and the parameters of welding was employed given in Table 2. No preheating was using for welding with Ni-base alloy filler wire. When welding process was completed, the samples were cute by Wire Electrical Discharge Machining (WEM) (type/ Smart DEM), to small specimens with dimension (50 × 10 × 10) mm, as shown in Figure 2.

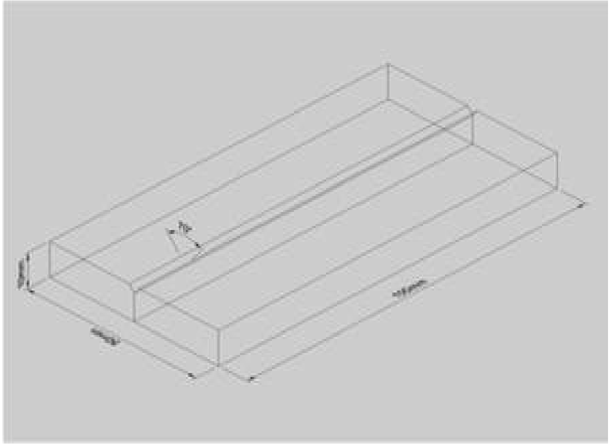

Figure 1: Schematic Configuration of V-Butt Welding Joint.

Figure 2: Specimen after Cutting

Table 1:- Chemical Composition of Base Metal and Filler Alloys

Base/Filler Metal %	Chemical Composition (% by Weight)									
	C	Cr	Ni	Mo	Mn	Si	Fe	Creq	Nieq	Creq/Nieq
AISI 410	0.127	11.94	0.2	0.0109	0.755	0.38	B	----	----	----
ERNiCrMo-3	2.28	15.83	67.36	7.95	----	0.42	0.95	24.41	68.26	0.35

Cr eq & Ni eq estimated from Shaeffler-Delong diagram assuming N=0.03wt%.

Table 2: Parameters of TIG Welding

Parameters	
Welding process	GTAW
Polarity	DCSP (direct current straight polarity)
Welding current	130 A
Welding voltage	70-80 V/Hz
Preheat temperature	------
Interpass temperature	------
Argon gas purity	99.999%
Shielding gas flow rate	6 $l.min^{-1}$
Backing gas flow rate	-------

II. Metallographic Procedure

Macro and microstructure studies were conducted along the cross section of specimens whose dimensions are (50 × 10 × 10) mm, which covering all the zones (base metals- HAZ-weld-metal) of the weldments. The cross-sectioned samples were ground by employing sheets emery of 320 to 2000 grit sizes on a Struers-127 polishing machine, and polished with diamond suspensions and alumina solution using the same machines. In order to a flat surface sectioned specimens firstly were mounted in acrylic and then etched by (0.5 ml Hcl+ 0.5 ml HNO_3 + glycerol). Standard metallographic procedures were carried out to examine the microstructure along the weldments using Nikon optical microscope with 5 mega pixel CCD camera into image pro software with the magnification of 5, 10, and 20X. The Vickers micro hardness test (HVS-1000) with diamond indenter was conducted on the polished mounted weld cross section, with load of 1Kg and duration time 15 seconds.

III. Line/Point, EDS and WDS Map/WDS Link analysis

Electron probe micro-analyzer (EPMA), Houses a JEOL 8200 Superprobe EPMA device at Microprobe Laboratory in the Department of Earth Sciences at the University of Dalhousie in Canada Country was used to complete these tests. The samples were prepared accordance with to ASTM E3-11 standard [7]. A set of points making along the weldments across base, HAZ and weld-metal regions, each of these points have been analyzed.

3. Results and Discussion

I. Micro-hardness Test Results

Typical micro-hardness profiles across the weldment 410 MSS/ ER NiCrMo-3 were showed in Figure 3. Results showed the variation in micro hardness profile depending on the dilution from the weld-metal zone and the base metal. The average hardness reached to HV 431.5 at HAZ compared to HV 166.5 and HV 229 at the weld-metal zone and the base metal, respectively. Thus, which clearly appeared the hardness is higher along HAZ region as compared with the base metal and the weld-metal zone.

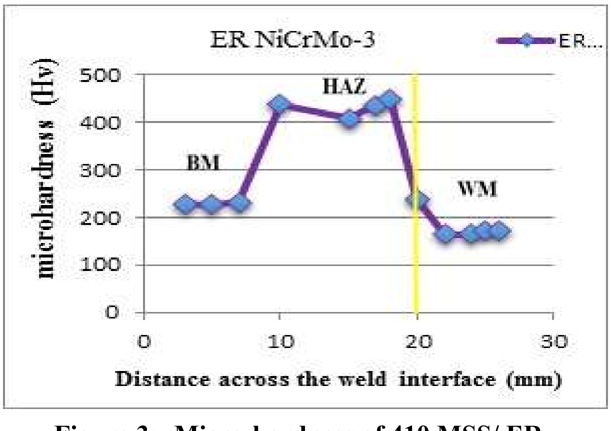

Figure 3:- Micro-hardness of 410 MSS/ ER NiCrMo-3 in State As-Welded

II. Micro-structure Examination along Weldments AISI 410/ER NiCrMo-3

In weld-metal zone of ER NiCrMo-3, nickel base alloy was found consisted of 67.36% Ni, 15.83% Cr and 7.95% Mo by weight, as mentioned in Table 1. The solidification mode was appeared to be fully austenitic (A) employing ER NiCrMo-3 filler metal due to very less Cr:Ni ratio which is equal 0.35% with moderate cooling rate and presence of austenite stabilizers (Ni eq 68.26%) in the filler wire. This was also corresponding in line with the Schaeffler. In addition, the full weld-metal zone revealed a granular structure consisting of dendritic and interdendrite structure, as shown in Figure 4. Line/point with EDS analysis along ER NiCrMo-3 illustrates in Figure 5. The results of analysis is confirmed the distribution of Ni element with high content along the weld-metal zone, whereas the Ni content were found along the weld zone in percentage (45.75, 53.54, 53.70, 52.63 and 47.22)%, this was proved that the austenite phase was solidified at the whole weld-metal zone. In addition, the results showed the presence of Mo, Nb and Ti along the weld-metal zone. Nb and Ti contents were found moving along weld-metal; both have ability to form carbides. Nb can stabilize the austenite phase at high temperatures and increase the solidification temperature range. While the existence of Mo makes the welds brittle at room temperature. Therefore, the solidification-cracking tendency was reduced. Solute redistribution of alloying elements in Ni- base alloys controlled the behavior of fusion zone (weld-metal) in Ni-base alloys. In addition, the segregation was occurred out through solidification of Ni-base alloys that resulted in a local variation in composition at the solidification subgrain level. In many alloys, segregation of alloy and impurity elements can lead to the formation of a second phase (or phases) at the end of solidification, as reported by Lippoled [8]. So that, X-ray image with magnification 10µm showed two phases: dendritic (dark region) and interdendrite (light region) phases, as shown in Figure 6(A). Line/point analysis with EDS analysis was done at dendritic and interdendrite, as shown in Figure 6(B and C). Results showed that the dendritic (dark region) at point Pt1 contained of Fe, Cr, Ni, Si and Mo in percentage (23.67, 19.96, 51.55, 0.26 and 4.33) %, respectively, While, the interdendrite (light region) at point Pt2 was found consisted of Fe, Cr, Ni, Si, Mo, Ti and Nb in percentage (14.62, 20.07, 52.54, 0.32, 8.46, 0.16 and 3.62) %, respectively.

The EDS analysis shown in Figure 6(C) at both regions confirmed that. It was observed from these analysis that the inter-dendrite phase enriched by Nb, since during solidification, Nb would be easily redistributed to in inter-dendritic regions, produces Nb enriched carbides, and moreover the amounts of Ni and Cr are not sufficient to dissolve Nb that could resulted in the formation of secondary phases, this was agreed with Mithilesh [5]. Liquid-solid interface and HAZ region are shown in Figure 7(A and B). Liquid-solid interface was liked plane between 410 MSS HAZ and ER NiCrMo-3 weld-metal zone. Weld-metal zone is predominantly columnar dendrites, which are perpendicular at the weld boundary, and grown towards the center of the molten pool (opposite to the direction of heat flow). Due to the exposition of HAZ region to thermal cycles during TIG process, the grain growth was occurred at HAZ AISI 410 martensitic, which was appeared tempered lath martensite with carbides. Line/point analysis at HAZ indicated that the region has richer amounts of Fe, Cr and C, and the elements such as Mn, Ni and Si were found to be in lesser amounts, as shown in Figure 8. The average C content along the HAZ was found 1.9%. X-ray image with magnification 500μm showed the presences of carbide particles (black points) distributed randomly at the HAZ region.

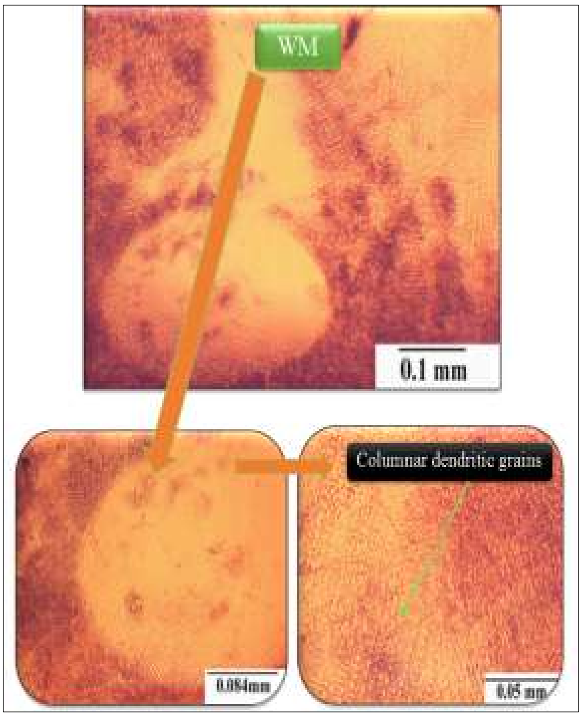

Figure 4:- Weld-Metal Zone for AISI 410 MSS/ ER NiCrMo-3 (As-Welded).

A)

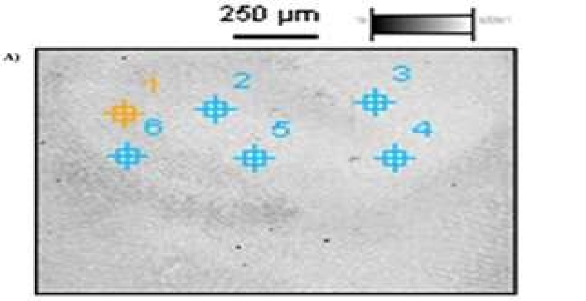

B) Weight %

	Al-K	Si-K	Ti-K	Cr-K	Fe-K	Ni-K	Nb-L	Mo-L
Base(209)_pt1	0.20	0.30	0.18	19.83	26.88	45.75	1.51	5.34
Base(209)_pt2	0.20	0.40	0.39	21.14	18.69	52.66		6.52
Base(209)_pt3	0.28	0.26	0.30	21.26	15.91	53.54	2.15	6.30
Base(209)_pt4	0.24	0.24	0.25	21.10	15.91	53.70	1.87	6.69
Base(209)_pt5	0.15	0.19	0.17	20.31	19.67	52.63	1.49	5.39
Base(209)_pt6	0.27	0.34	0.22	20.27	23.63	47.22	2.02	6.04

c)

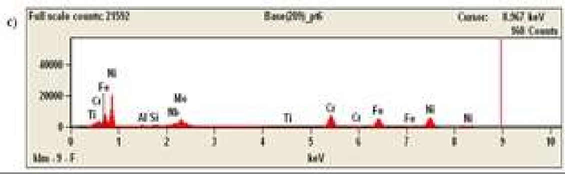

Figure 5:- A) Line analysis, B) Point analysis and C) EDS Analysis at the Weld-Metal Region for AISI 410/ ER NiCrMo-3 (As-welded)

A)

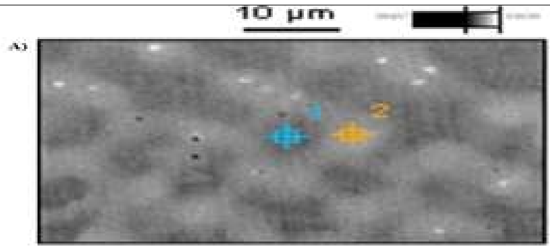

B) Weight %

	Al-K	Si-K	Ti-K	Cr-K	Fe-K	Ni-K	Nb-L	Mo-L
Base(210)_pt1	0.23	0.26		19.96	23.67	51.55		4.33
Base(210)_pt2	0.21	0.32	0.16	20.07	14.62	52.54	3.62	8.46

c)

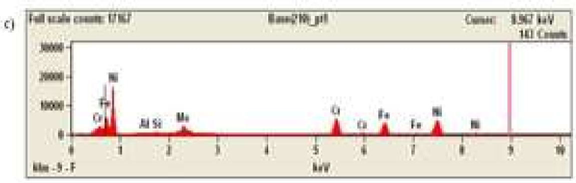

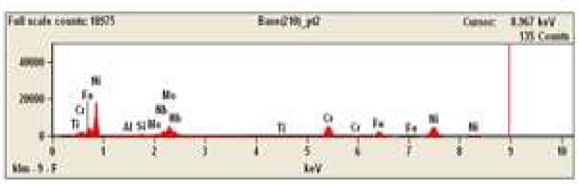

Figure 6:- A) Line analysis B) Point analysis and C) EDS Analysis at the Dendritic and interdendritic Region for AISI 410/ ER NiCrMo-3 (As-welded).

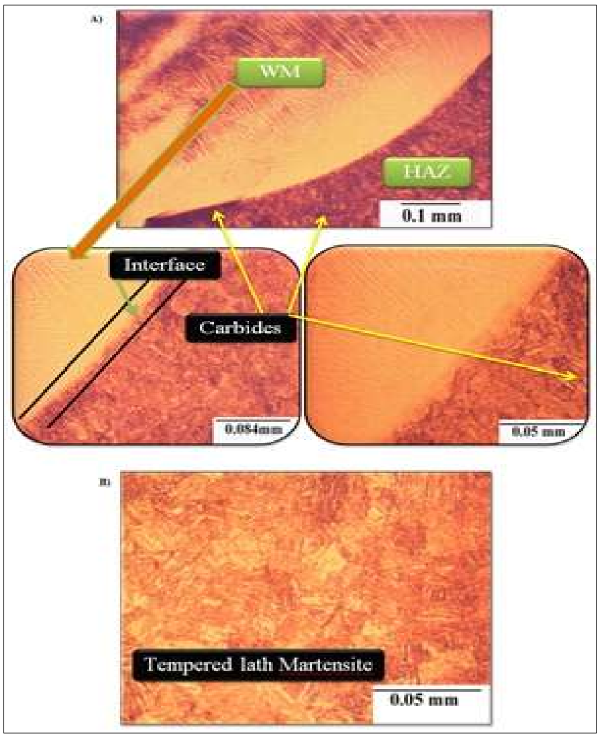

Figure 7:- A) Liquid-Solid Interface B) HAZ Affected Zone for AISI 410 MSS/ ER NiCrMo-3 (As-Welded).

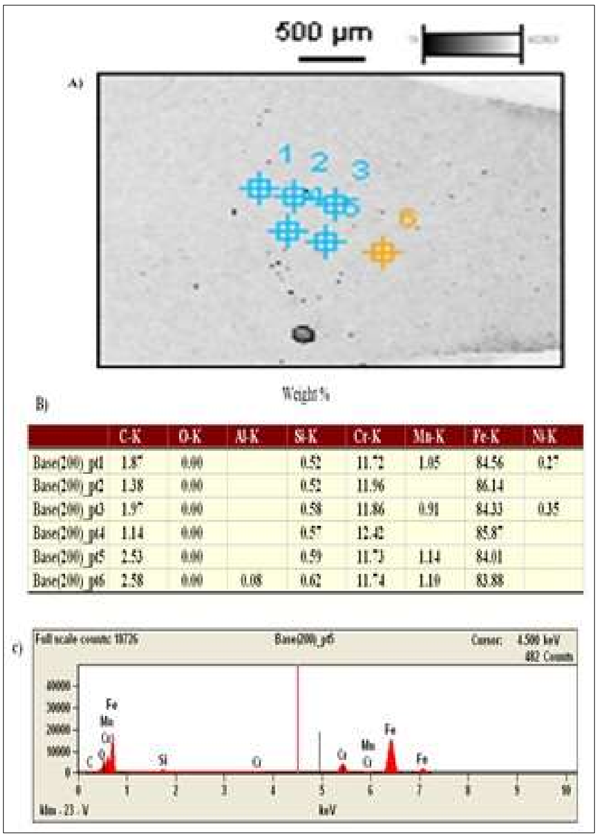

	C-K	O-K	Al-K	Si-K	Cr-K	Mn-K	Fe-K	Ni-K
Base(200)_pt1	1.87	0.00		0.52	11.72	1.05	84.56	0.27
Base(200)_pt2	1.38	0.00		0.52	11.96		86.14	
Base(200)_pt3	1.97	0.00		0.58	11.86	0.91	84.33	0.35
Base(200)_pt4	1.14	0.00		0.57	12.42		85.87	
Base(200)_pt5	2.53	0.00		0.59	11.73	1.14	84.01	
Base(200)_pt6	2.58	0.00	0.08	0.62	11.74	1.10	83.88	

Figure 8:- A) Line analysis, B) Point analysis and C) EDS Analysis at the HAZ Region for AISI 410/ ER NiCrMo-3 (As-welded).

III. Diffusion Elements by WDS MAP/WDS LINK:

WDS Map/WDS Link analysis to explain chemical quantitative for elements along the weldement AISI 410/ER NiCrMo-3 is illustrates in Figure 9 and 10. Whereas WDS Map in Figure 9 (A), confirmed HAZ region consisted of major elements as Fe, Cr, Si, C and O. while WDS link in Figure 10 (A) appeared Mo was moved in straight line along base and HAZ regions. This is due to dilution from weld-metal region. Hence, average Fe, Cr, Si and C along HAZ region near from the interface was found (4175-4183), (976-962), (76-75) and (59-71), respectively. This was supported the hardness profile in Figure 3. It can be noted increased hardness along HAZ region. Due to, carbon has coefficient diffuse much more than chromium and iron at a ferrite structure (BCC) than at austenitic phase (FCC), thus C was faster than rest elements to union with Cr and Fe to form carbides, as reported by Erich Folkhard and Fadhil et.al. [9, 10]. Thus, large amount of carbon was aggregate at HAZ region. In addition, WDS Map in Figure (9) evidenced Fe and Cr was moved toward weld-metal region. Figure 9 (B) and 10 (B) viewed WDS Map/WDS Link analysis viewed the average and movement along the weld-metal regions. Whereas average Fe, Cr, Si, C, Mo, Nb, Al and Ni along weld-metal were found 814, 909, 54, 53, 16, 54, 25 and 649, respectively. Thus, it can be noted Cr was continue raised along HAZ and weld-metal, while Fe reduced at weld-metal region. Ni element appeared along weld-metal region with value 649; this supported Ni was substituted with Fe element. Due to Fe has atomic radio similar to Ni (whereas, Fe has 0.3% approximate atomic size difference compared with nickel), this results increased strength. This was agreed with [6], the author has reported the elements such as Fe, Co and Cr can substitute by Ni. Those elements with similar atomic radii to Ni have k values that are close to unity. In addition, Nb element did not appear at the base and the HAZ region as compared to weld-meta zone. Due to the Nb was non-existent movement in α – ferrite phase, while it has less movement at γ – austenite phase at the ambient temperature as compared with the rest elements, whereas the Nb has a coefficient of diffusion 7.5×10^{-5} (m2/sec) and activation energy 264 KJ/mol at γ-Ni (FCC), according to Lippoled [8]. In addition, it can be noted from Figures 10 intensity of Ti, Nb, Mo and Al was increased along the weld-metal region. Figure 9 (c) and 10 (c) illustrate the average and movement of elements at the other side, whereas average Fe, Cr, C and Si on HAZ region at other side was found in rang (4192-4196), (965-953), (53-43) and (80-76). While, it was observed Si element continued moving from base, HAZ (H1) near the liquid-solid interface toward the weld-metal zone with approximately the same level. Due to, Si has the same coefficient diffusion in austenite phase and ferrite matrix at ambient temperature.

A)

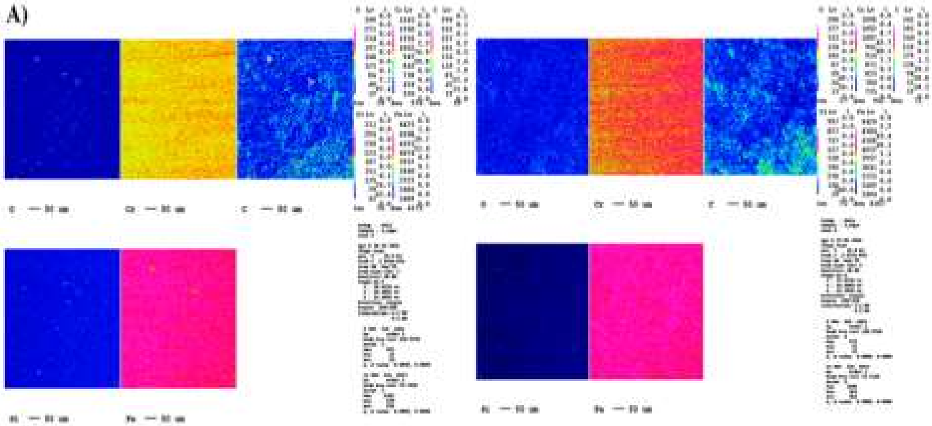

B)

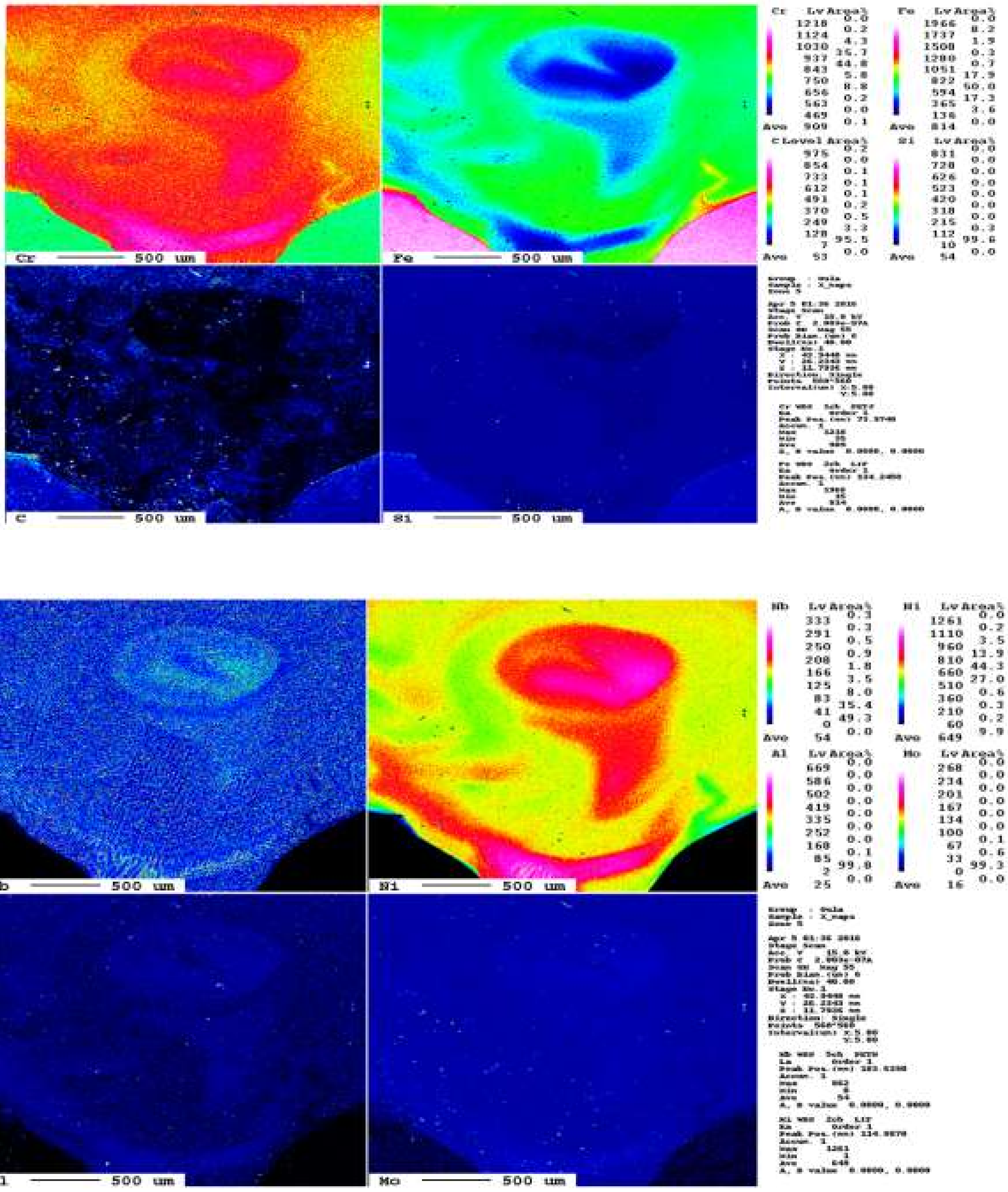
Cr 500 um
Fe 500 um
C 500 um
Si 500 um
Nb 500 um
Ni 500 um
Al 500 um
Mo 500 um

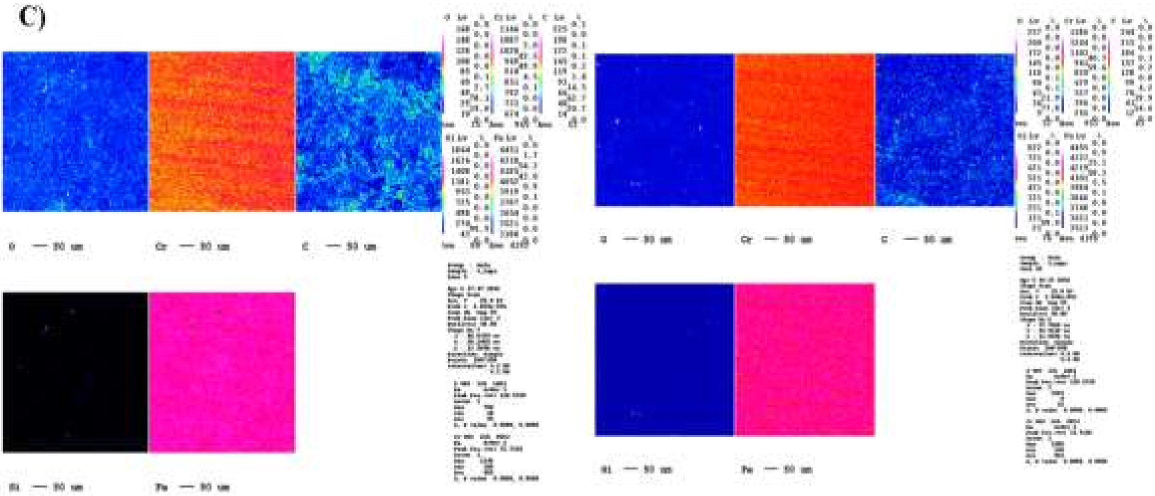

Figure 9: WDS MAP A) HAZ Region B) Weld-Metal Region C) HAZ Region at other side for Weldment AISI 410MSS/ ER NiCrMo-3 (As-Welded)

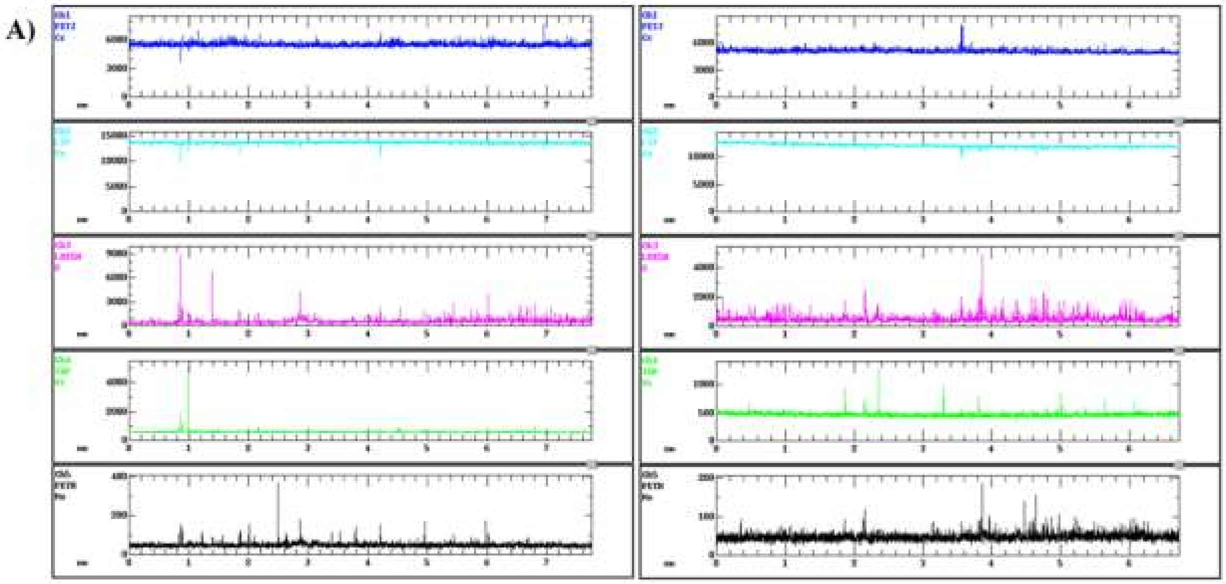

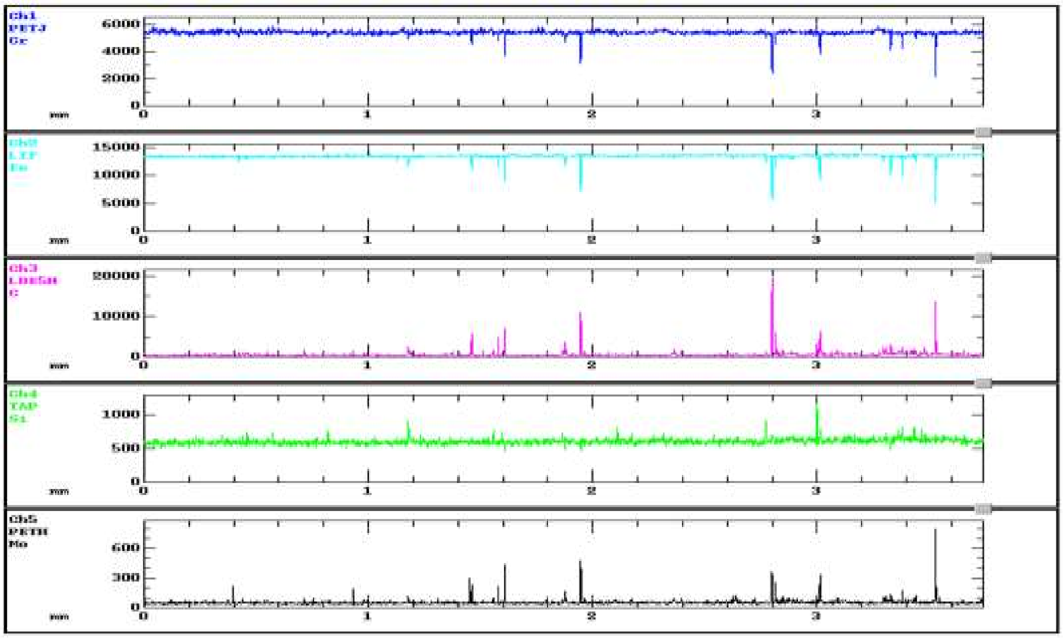

B)

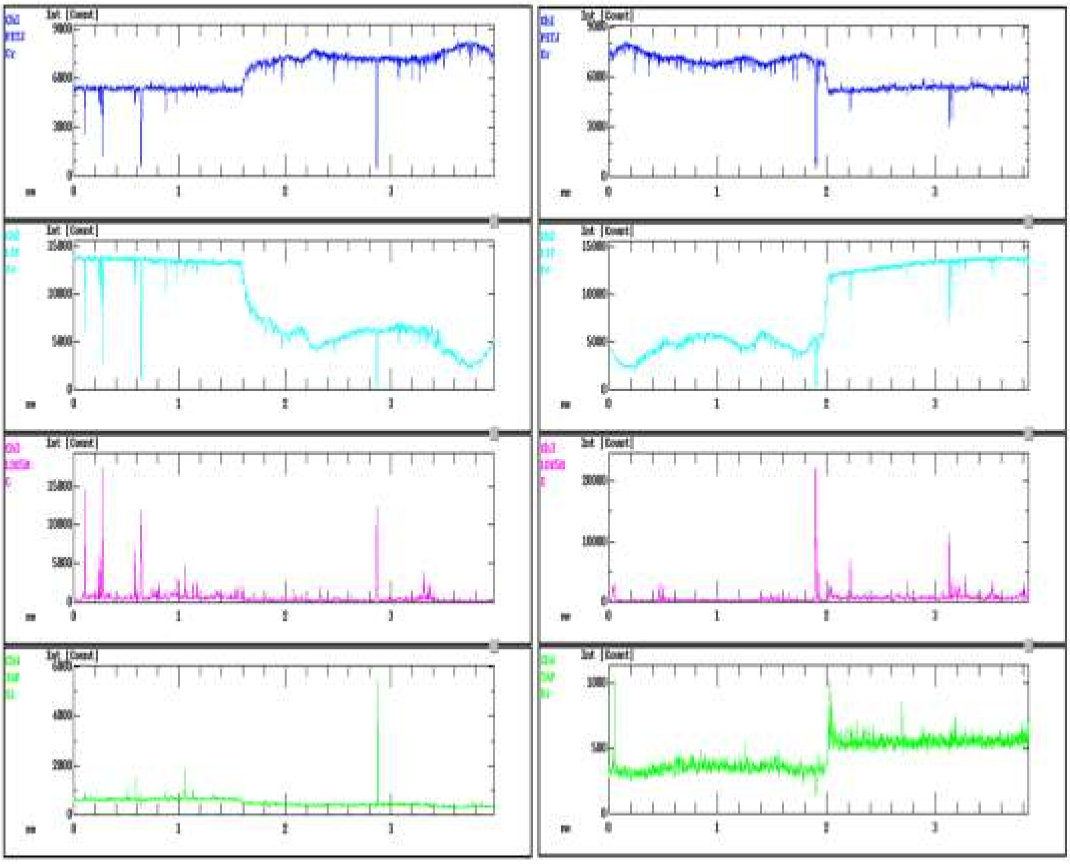

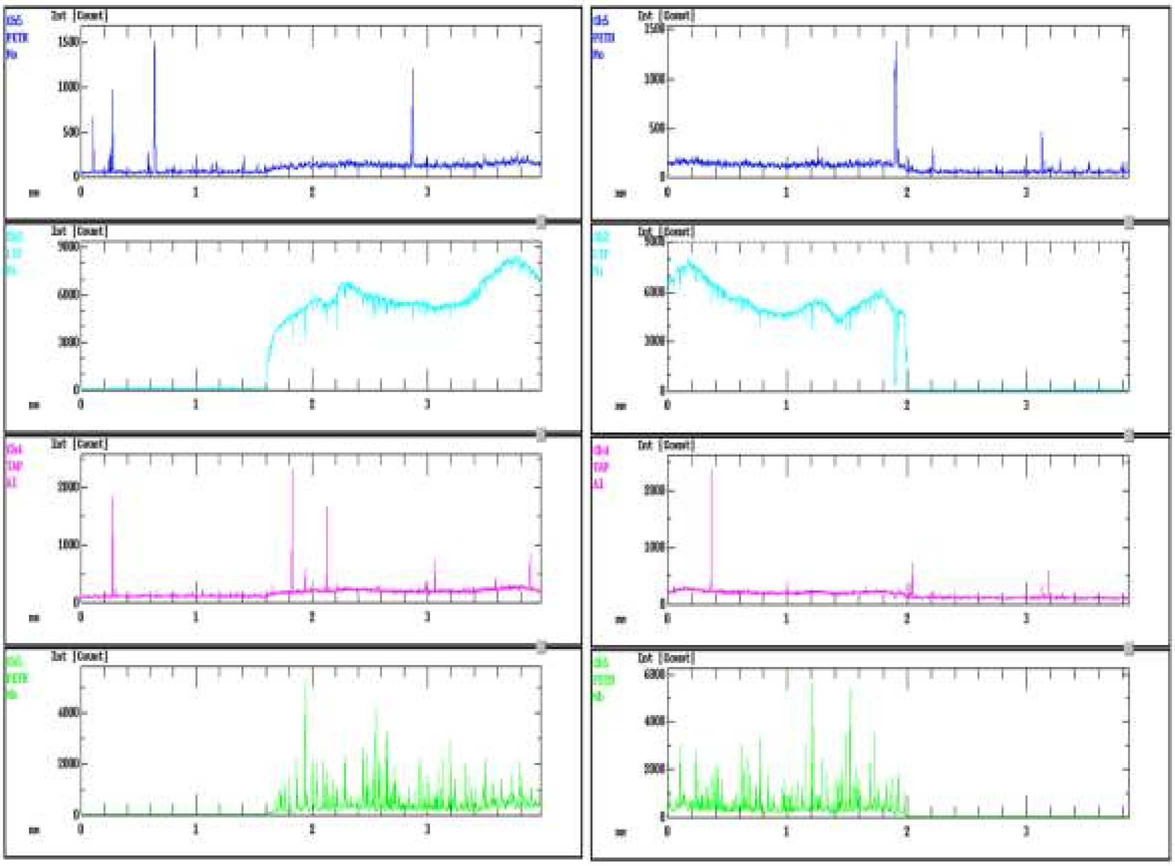

C)

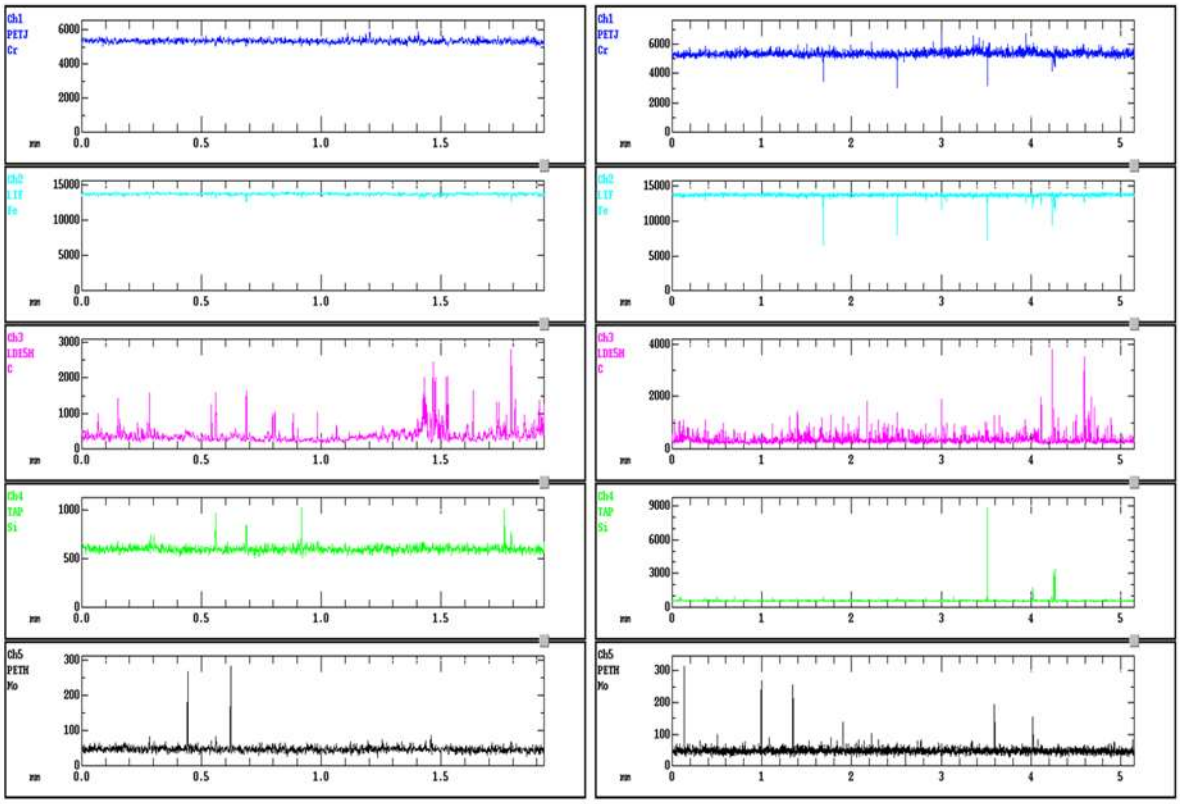

Figure 10: WDS Link for A) HAZ Regions B) Transition and Weld-Metal Regions C) Along HAZ at other Side for Weldment AISI 410MSS/ ER NiCrMo-3 (As-Welded).

4. Conclusion

- Sound welds of 410 MSS blade steam turbine could be obtained from GTA welding process using ER NiCrMo-3 filler wires.
- After welding process, the solidification mode was appeared to be fully austenitic (A) by employing ER NiCrMo-3 metal due to Cr:Ni ratio very less with the moderate cooling rate and the presence of austenite stabilizers (Ni eq 68.26%) in the consumable filler wire.
- X-ray image showed two phases along the ER NiCrMo-3: dendritic and interdendrite phases. Chemical composition showed dendritic contained elements of Fe, Cr, Ni, Si and Mo, respectively. While, the interdendrite was found consisted of Fe, Cr, Ni, Si, Mo, Ti and Nb, respectively.
- Carbon elements aggregated at HAZ region close to interface to form carbides in different form as $M_{23}C_6$. Fe element good moved toward weld-metal region than Ni and Cr elements.
- Ni substitution by Fe in ER NiCrMo-3 weld-metal.
- Diffusion elements from base toward HAZ regions with approximately the same average. Ni, Mo, V and Mn have very low coefficient diffusion at ambient temperature.
- Si element has same coefficient diffusion at base, HAZ and weld-metal regions. In addition, Nb was non-existent movement in α-ferrite phase, while it has less movement at γ-austenite phase at the ambient temperature.

References

[1] S.K. Albert, C.R. Das, V. Ramasubbu, A.K. Bhaduri, S.K. Ray and Baldev Raj, "In Situ Repair Welding of Steam Turbine Shroud for Replacing a Cracked Blade," Journal of Materials Engineering and Performance, Vol. 11, No. 3, pp. 243-249, 2002.

[2] D. Goutam, G.C. Sandip, S.K. Ray, K.R. Ashok, K.D. Swapan and K.B. Deepak, "Turbine Blade Failure in a Thermal Power Plant," Engineering Failure Analysis. Vol. 10, pp. 85–91, 2003.

[3] A.K. Bhaduri, T.P.S. Gill, S.K. Albert, K. Shanmugam and D.R. Iyer, "Repair welding of cracked steam turbine blades using austenitic and martensitic stainless-steel consumables," Nuclear Engineering and Design, Vol. 34, No. 23, 249-259, 2001.

[4] M. Divya, C.R. Das, S.K. Albert, V. Ramasubbu, A.K. Bhaduri and P. Sivaraman., "In-situ weld repair of cracked shrouds of turbine and characterization of the weld joint," Ommi, 1-11, 2011.

[5] P. Mithilesh, D. Varun, Ajay Reddy Gopi Reddy, K. Devendranath Ramkumar, N. Arivazhagan and S. Narayanan. "Investigations on Dissimilar Weldments of Inconel 625 and AISI 304," Elsevier, Procedia Engineering, Vol. 75, pp.66-70, 2014.

[6] M. Arivarasua, D.R. Kasinatha, A. Natarajan, "Effect of continuous and pulsed current on the metallurgical and mechanical properties of gas tungsten arc welded AISI 4340 aeronautical and AISI 304L austenitic stainless steel dissimilar joints," Materials Research, Vol. 18, 59-77, 2015.

[7] ASTM International Standards, "Standard guide for preparation of metallographic specimens," 2011

[8] C.John, Lippold, N.John Dupont and D.Samuel Kiser, "Welding Metallurgy and Weldability of Nickel-Base Alloys," John Wiley & Sons, Inc., New Jersey, 2009.

[9] F. Erich, "Welding Metallurgy of Stainless Steels," Springer-Verlag/Wien, New York, 1988.

[10] A.H Fadhil, S.A. Emad, K. H. Abbas, H. A. Olaa, "Welding Procedures ofTurbine Blades by Using ER309L Austenitic Filler Wire," Engineering and Technology Journal, Vol.35,part A, No. 1, 2017.

Author(s) biography

Assist. Prof Dr. Emad. S. AL-Hassani is interested with metal engineering. He is working in the Materials Engineering Department, University of Technology, Iraq. He has been working on various aspects related to shape memory alloys and biomedical metals.